30th NENE 2021
September 6 - 9
BLED-SLOVENIA
International Conference Nuclear Energy for New Europe

Assessment of Power Deposition on Plasma Facing Components Inside WEST Tokamak

Matic Brank[1], Mehdi Firdaouss [2], Marie-Helene Aumeunier [2], Gregor Simič [1], Leon Kos [1]

[1] Faculty of Mechanical Engineering, University of Ljubljana
Aškerčeva 6, 1000 Ljubljana, Slovenia
matic.brank@lecad.fs.uni-lj.si
gregor.simic@lecad.fs.uni-lj.si
leon.kos@lecad.fs.uni-lj.si

[2] Institute for Magnetic Fusion Research, CEA,
Cadarache, 13115 Saint-Paul-lez-Durance, France
mehdi.firdaouss@cea.fr
marie-helene.aumeunier@cea.fr

ABSTRACT

Assessment of plasma power deposition with the use of magnetic field-line tracing on tokamak plasma facing components is important in order to provide thermal loading of critical components in the fusion reactors. Such analysis can provide insight into PFC design and can improve the durability and safety of nuclear fusion reactors.

This article describes a benchmark performed between two magnetic field-line tracing (FLT) codes, PFCFLUX [1] and SMITER [2]. The code PFCFLUX (Plasma Facing Components Flux) has been developed for heat flux calculations on those components, including shadowing effects. SMITER is a graphical user interface (GUI) framework, built around SMARDDA [3] kernel for magnetic field-line tracing and power deposition mapping on tokamak plasma-facing components (PFC) in the full 3-D CAD geometry of the machine. The main purpose of the benchmark presented here is the evaluation of the power deposition on the poloidal limiters (high and low field sides) and the divertor targets of WEST tokamak. Magnetic coils of WEST have been added to confine the originally circular plasma into and ITER-like ”D”-shape. As one of the main testing tokamaks for ITER, it is thus also suitable to provide assessment of heat loads on plasma facing components inside WEST.

The input parameters to field-line tracing codes are the target geometry, shadowing geometry and 2-D equilibrium data. Target geometry describes the geometry where the power fluxes will be assessed. Field-lines are traced back from the target triangles into the scrape-off layer region. Shadowing geometry acts as a shadow. If field-lines of a target triangle hit the shadowing geometry, then this triangle is considered non-wetted. If the field-line does not hit anything after a user-defined maximum distance, then the target triangle is considered wetted, and power deposition can be calculated based on the provided heat flux profile. Equilibrium data contains information about magnetic field fluxes defined in R-Z space and are assumed to be axisymmetric in the toroidal direction.

1 INTRODUCTION

The plasma-facing components (PFC) for fusion reactor design need to sustain high heat fluxes coming from the plasma in order to prevent local melting of the material which could endanger the safety and operation on fusion reactor. A key utility in such design is field-line tracing for different magnetic field equilibria which allows the definition of component front surface shaping. This design phase deploys both analytic theory [4] and the field-line tracing simulations. In addition, the critical issue of management and control of PFCs in actively cooled devices (such as WEST and ITER) requires attention from operators. To facilitate the development of such control algorithms for protection of beryllium and tungsten PFCs [5], the examination of plasma power deposition with FLT is of huge importance.

2 DEVELOPMENT AND METHODOLOGY

The main purpose of PFCFlux during its development phase was to decrease large computational times from other FLT tools, such as Tokaflu [6]. It was built on more modern hardware than its predecessors using faster algorithms and parallelisation, meaning all CPU threads are used for this application.

Besides large computational times, the difficulty also arises from the setup of simulation case, which usually involves different commercial packages starting with CAD model preparation and meshing of CAD models. CAD model defeaturing is necessary to avoid unnecessary details. Defeatured models also result in higher quality meshing and cause fewer numerical problems in smiluations. Here, the SMITER field-line tracer was developed with sophisticated graphical user-interface (GUI) which enables user to prepare CAD models, meshes and multiple FLT studies within one framework. Multiple studies can be run in parallel, thus reducing not only computational time, but also user's time in terms of preparing and running FLT simulations.

The main goal of every field-line tracer is to calculate shadowing pattern and parallel heat flux on a given object for a magnetic configuration. The shadowing calculation consists of following the magnetic field-lines issued from the meshed object (nodes in PFCFlux and triangle barycenter in SMITER) - named *target* objects. In both solvers, the assumption is made that the particles follow the magnetic lines perfectly. The difficulty lies in the efficiency of calculation, because the number of nodes and surrounding objects are potentially very large. In PFCFlux, the algorithm relies on a 2nd order Runge-Kutta (RK2) pattern, while SMITER uses Runge-Kutta-Fehlberg schemes. The intersection of trajectories with surrounding objects, discretized with triangles (usually named *shadowing* objects) is ensured by Möller-Trumbore algorithm. This intersection test is the most demanding task in terms of computational time, so octree approach is used in both solvers: the space containing shadowing meshes is partitioned into boxes. The intersection test is done only for the triangles encapsulated in the same box as the field-line, thus allowing additional speed-up gain.

2.1 Field-line tracing

Magnetic field and magnetic flux are provided from different equilibrium codes, such as EFIT [7] or DINA [8]. The standard field-line equation is given as

$$\dot{\mathbf{x}} = \frac{d\mathbf{x}}{dt} = \mathbf{B}(\mathbf{x}) \tag{1}$$

Eq. 1 denotes differentiation of field with respect to pseudo-time t. The term "pseudo-time" refers to solving the steady-state solution of Eq. 1. The magnetic field **B** is assumed to be axisymmetric (independent of toroidal angle ψ). Full 3-D configuration of magnetic field due to misalignment of coils is also possible but will not be presented in this paper.

2.2 Power deposition model

The calculation of parallel heat flux comes from the knowledge of the power repartition in SOL which is the problem of physics and is an ongoing field of research. Multiple models exist, such as Eich model, double exponential and single exponential decay. Assuming single exponential decay loss across the SOL, starting from the first separatrix (diverted configuration) or last closed flux surface (limiter configuration), the parallel heat flux is defined as

$$q_{||}(R) = q_{||,omp} \exp\left(-(R - R_m)/\lambda_m\right) \tag{2}$$

Here, $q_{||,omp}$ is parallel heat flux at midplane, $R_m[m]$ is radial position of midplane, $\psi_m[W_b]$ is magnetic flux at midplane and $\lambda_m[m]$ is decay length. Radial distance from the separatrix can also be expressed in terms of flux coordinates

$$R - R_m = \frac{\psi - \psi_m}{R_m B_{pm}} \tag{3}$$

Here, B_{pm} is poloidal component of magnetic field **B** at midplane. The power density, deposited on the surface with normal **n**, can then be expressed as

$$q_{\perp}(\psi) = \frac{F P_{loss}}{2\pi R_m \lambda_m B_{pm}} \mathbf{B.n} \exp\left(-\frac{(\psi - \psi_m)}{\lambda_m R_m B_{pm}}\right) \tag{4}$$

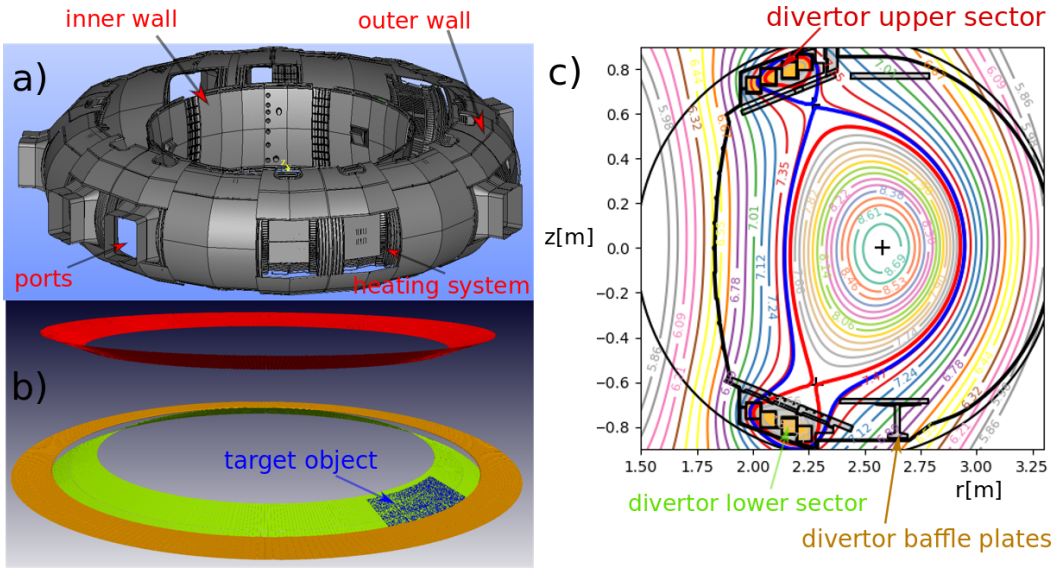

Figure 1: (a) CAD model of plasma-facing components of WEST tokamak. (b) Case setup for field-line tracing simulation with three distinctive shadows: divertor lower and upper section and divertor baffle plates. Target is given as a portion of divertor lower sector. (c) Cross-section of tokamak WEST with geometry and magnetic flux contours.

In Eq. 4, $F = 1/2$ is the factor to allow for an equal amount of power being lost in the opposite directions. Parameters ψ_m, R_m, B_{pm}, **B** and **n** are evaluated through interpolation of

magnetic data on meshing objects, so $q_\perp$ is only determined through SOL power P_{loss} and decay length λ_m. More detailed explanation on how these equations are derived is given in [3].

3 FLT SIMULATIONS

A benchmark case between both codes was prepared for diverted configuration in WEST tokamak. Plot of magnetic flux configuration can be seen in Fig. 1. FLT solver first processes given magnetic input and mesh objects. As noted, for the single exponential decay length, only two parameters are given as

- **Power loss**: $P_{loss} = 3MW$
- **Decay length**: $\lambda_m = 0.01m$

After reading the magnetic configuration data, the solver will map magnetic field and magnetic flux components to target objects.

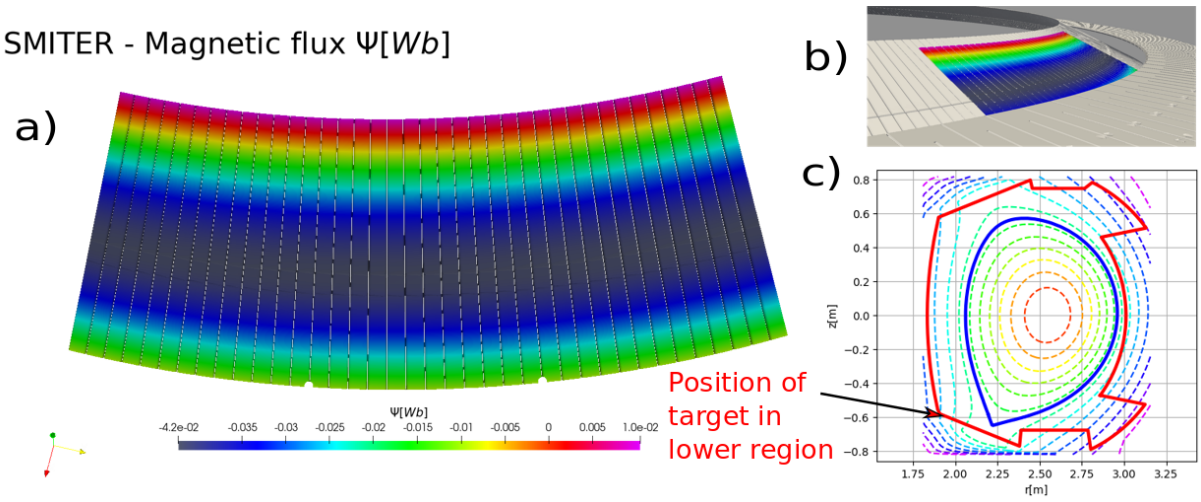

Figure 2: (a) Distribution of magnetic flux on target. (b) Side view of target and shadow (c) First wall contour (red) and first separatrix (blue) with contour plot of magnetic flux. Position of target in lower region is displayed as well.

Magnetic flux of SMITER mapping can be seen in Fig. 2a. One can notice that the maximum value of magnetic flux appears at the top of the tiles, which corresponds well to the plot given in Fig. 2c. Similar results are obtained with PFCFlux. The maximum relative error difference between two solvers is 0.2%, so one can conclude that mapping of magnetic flux to the target triangles is almost identical.

The field-line tracing results are shown in Fig. 3. The choice of maximum length of the field-line is somehow arbitrary, but can depend on different SOL conditions. In terms of edge localized mode (ELM) effect, shorter field-lines can be chosen in order to account for the balance between characteristic parallel and perpendicular ELM filament transports, which results in larger "wetted" area i. e. the field-line is terminated before it can reach the intersection triangle. In benchmark presented here, field-line lengths were traced roughly up to $L_{FLT} \sim 67m$ or until they reached the edge of the computational domain. Regarding values of L_{FLT}, the plot can be divided roughly in five regions (see Fig. 3a) with distinctive lengths. In Fig. 3b,the intersection between field-line from region 5 (purple) and triangle on divertor baffle plate is

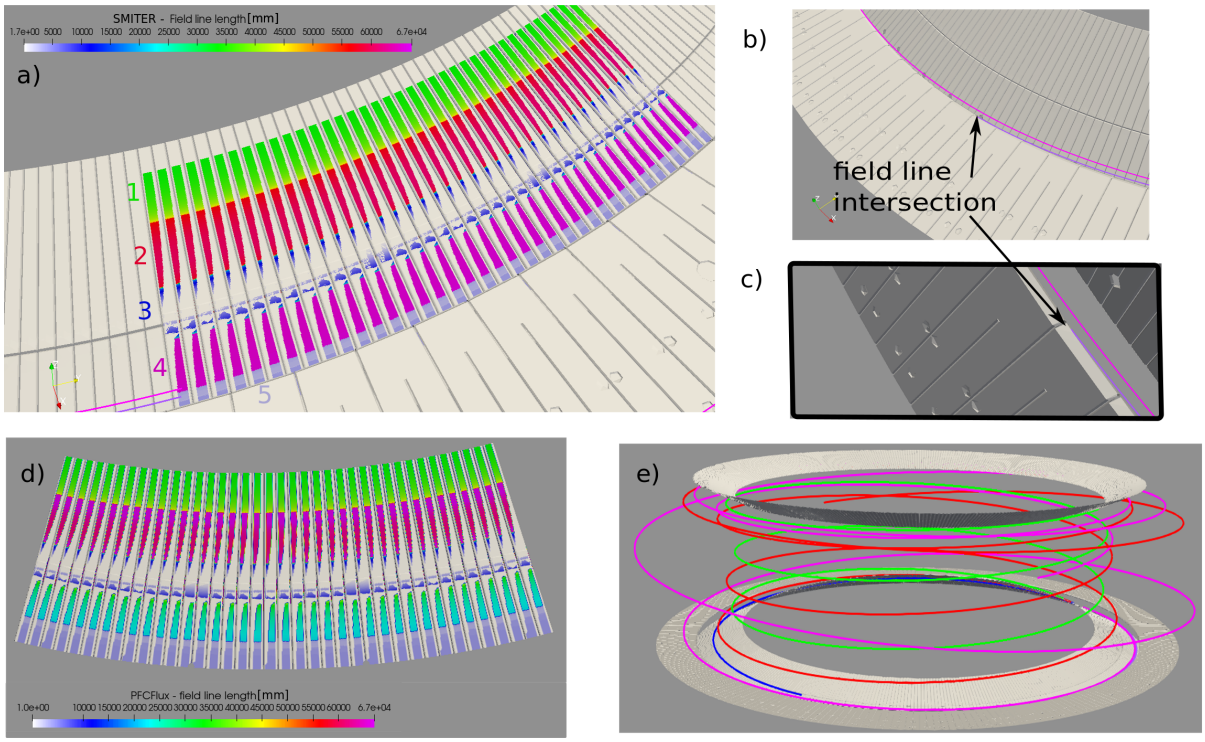

Figure 3: (a) Field-line lengths for target triangles, plotted on top of shadowing geometry. Five distinctive regions can be seen from the plot. (b) Front view of intersection between shadowing triangle and traced field-line (purple color). Note the field-line from region 4 (pink color - length of field-line is $L_{FLT} \sim 65m$) which is not intersected by any triangle and thus continues its path. (c) Side view of triangle-field-line intersection. (d) Plot of field-line lengths in PFCFlux. Note that intersected regions have the same length (regions 1, 3 and 5), while the regions with no intersection differ in values. (e) Full path of field-lines from all five regions. Note how the field-lines are correlated to magnetic field in the tokamak.

calculated and field-line is terminated. Meanwhile the field-line from region 4 (pink color) is not intersected by any triangle and thus continues its path until it reaches the value of $L_{FLT} = 67m$ and is terminated. Its triangle is then considered "wetted". Plot of field-line lengths in PFCFlux shows that intersected regions have the same lengths (regions 1, 3 and 5), while the regions with no intersection differ in values. Here, different field-line termination criteria was chosen. Regions, intercepted by shadowing triangles, keep the same values as in SMITER, while others are terminated earlier. The wetted area is still calculated correctly. As mentioned, this does not affect calculation of power deposition on PFCs, since the chosen single exponential omp $q_{||}$ profile is not dependent on length of field-lines. In specific cases such as calculation of ELM profiles, the termination criteria of field-lines can play a role on how the parallel heat flux $q||$ is calculated. The theory on how this is done is explained in more detail in [9]. Exemplary studies explaining the process of such simulation can be found in [10] [11]. The paths of field-lines are somehow expected since it is based on the configuration of the magnetic field and flux. They are moving from lower divertor regions and do multiple circles around the tokamak to the upper divertor region of the tokamak. Termination and lengths of all regions can be seen in Table[1].

From calculation of connection lengths the FLT solver can thus deduce wetted area which is shown in Fig. 4. Note that wetted area corresponds to triangles whose field-lines were not intercepted by shadowing triangles. Meanwhile triangles whose field-lines were intercepted by shadowing objects are suppressed and are not used in power deposition calculation. The

Table 1: Field-line lengths - refer to Fig. 3a

region	$\sim L_{FLT}[m]$	observation
1	32	Field-lines intersect upper divertor region
2	55	Field-lines are not intercepted by shadowing objects
3	12	Field-lines intersect lower divertor region
4	65	Field-lines are not intercepted by shadowing objects
5	5	Field-lines are intercepted by baffle geometry

calculation of impact angle between triangle and its field-line is also of essence. The impact angle will determine power deposition $q_{\perp}$ on the triangle barycenter (or node, which is the case in PFCFlux). This power deposition is the fraction of parallel heat flux $q_{||}$, derived through previously explained exponential profile. Note that angle is not directly seen in the Eq. 4, but it is expressed through dot product of magnetic field vector $\mathbf{B}[T]$ and normal $\mathbf{n}$ (both defined in barycenter/node of triangle). Plots of angles are shown in Fig. 4. The results are as expected. The angle on sides of tiles is $\sim 80^{\circ}$ because the triangle is almost perpendicular to magnetic field. On the front side, the values are very low on top of the bump located in the middle of each tile, because the bump surface is lifted towards the plasma center. Maximum relative difference in angles between both solvers is around 2.5%. Note the red frame around wetted area on each tile. The difference comes in the calculation of filed line intersection. Field-lines of these triangles were not intercepted in SMITER, while PFCFlux calculated the intersection with shadowing triangles and assumed $\alpha_{PFCFlux} = 0$. This is a clear difference in calculation between two codes which shows some level of inaccuracy.

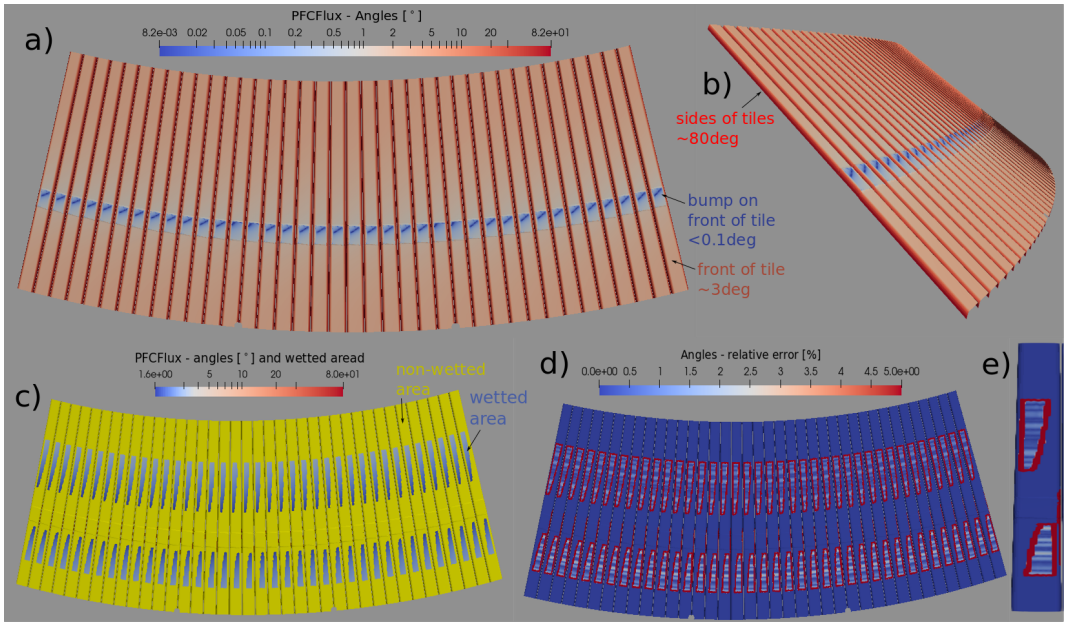

Figure 4: (a) Size of angle between incoming field-line and triangle surface. (b) Side view of target with angles. (c) Result of field-line tracing. Yellow color marks triangles whose field-lines were intercepted by shadowing triangles. Wetted area is marked with plot of angles between field-lines and triangle surface. (d) Relative error in angles between both FLT solvers. Note the red frame around wetted area region. (e) Detailed view of relative error on first tile.

The maximum heat load obtained with PFCFlux on the front surface is $q_{PFC} \sim 4.5 MW/m^2$, while SMITER computes $q_{PFC} \sim 4.66 MW/m^2$, which yields a difference of 3.5%. The dif-

ferences in surface heat load errors increase with the distance from the separatrix but remain roughly within 5% between the two codes. The red frame around wetted area which corresponds to large percentage differences is, as explained before, difference in wetted area between the two codes and can be ignored in terms of power deposition comparison. Other difference can be observed as sharp surface variations. Closer examination reveals red bands which are caused by PFCFlux averaging surface normals from nodes while SMITER computes normals from a single triangle. It is observed that SMITER is thus more accurate on edges and has some oscillations found on normals on smooth surfaces. More details on this can be found in discussion on surface accuracy in Section II-C3 and Support Section II in [3].

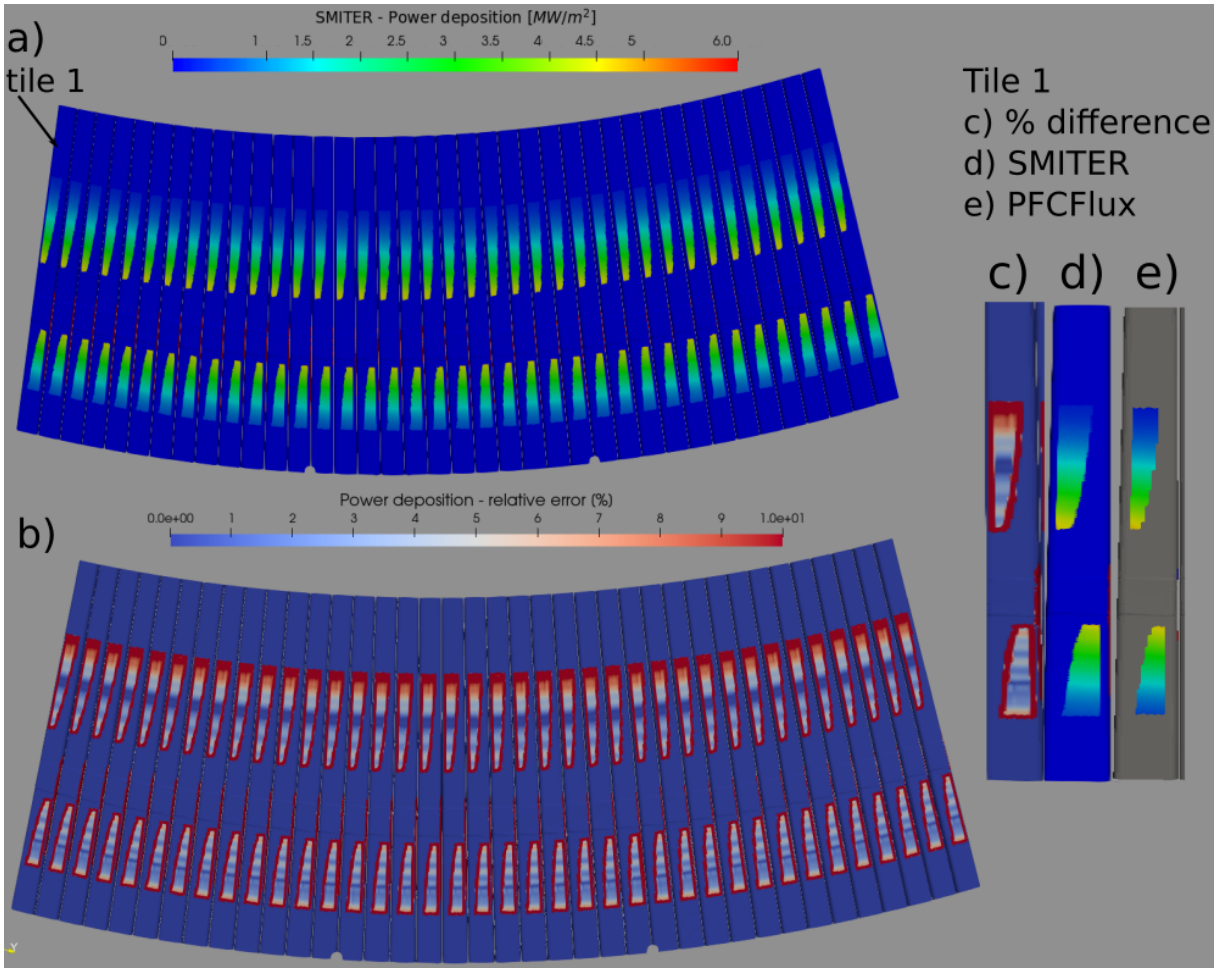

Figure 5: (a) Power deposition result in SMITER. (b) Relative error difference between two codes. (c)(d)(e) Detailed plots of first tile.

4 CONCLUSION

Both SMITER and PFCFlux have been extensively verified against experimental data [12] and other numerical solvers and validated for both divertor and limiter configuration. Here, both FLT solvers are presented and a benchmark is performed which shows the consistency in results between both solvers. Although certain dfferences exist, such as numerical methods for field-line tracing calculation, difference in evaluation of parameters on nodes (PFCFlux) vs. barycenters (SMITER) of triangles, one can conclude from the work presented here and numerous other papers, referenced in this paper, that both solvers are capable of solving FLT

problems. PFCFlux is already widely used at CEA for calculation of thermal power deposition and is already used in production of synthetic diagnostic signals for testing of WEST tokamak. SMITER is extensively used at ITER where it is actively deployed for the development of simplified real time wall heat flux control algorithms [5] and is expected to play an important role in the production of synthetic diagnostic signals for the testing of ITER systems being prepared for PFC power flux control and monitoring.

REFERENCES

[1] M. Firdaouss et al., "Modelling power deposition on the JET ITER like wall using the code PFCFLUX", Journal of Nuclear Materials, 438, 2013, 536–539

[2] L. Kos et al., "SMITER: A field-line tracing environment for ITER", Fusion Engineering and Design, 03, 2019, DOI: 10.1016/j.fusengdes.2019.03.037

[3] W. Arter, V. Riccardo, G. Fishpool, "A CAD-based tool for calculating power deposition on tokamak plasma-facing components", IEEE Trans. Plasma Sci. 42 (2014) 1932–1942.

[4] P. Stangeby, "Analytic expressions for shaping analysis of the ITER outer wall", Nucl. Fusion 51 (2011) 103015

[5] H. Anand, R.A. Pitts, et al., "Implementation of 3-D effects of the plasma-facing components in a 2-D real-time model based approach for wall heat flux control on ITER", 27th IAEA FEC, Gandhinagar, India, 2018, pp. 1–8 (EX/P7-24).

[6] R. Mitteau et al., J. Nucl. Mater. 313–316 (2003) 1229

[7] O. Meneghini et al 2015, "Integrated modeling applications for tokamak experiments with OMFIT", Nucl. Fusion 55 083008

[8] R.R. Khayrutdinov and V.E. Lukash, "Studies of Plasma Equilibrium and Transport in a Tokamak Fusion Device with the Inverse-Variable Technique". Journal of Computational Physics, 109(2):193-201, 1993.

[9] M. Kocan, et al., "Modelling ELM heat flux deposition on the ITER main chamber wall", Journal of Nuclear Materials, 709-713. doi:101016/jjnucmat201411130

[10] H. Anand, et al., "A framework for the assessment and control of ITER main chamber heat loads" Nucl. Fusion, 60 (2020), Article 036011

[11] M. Brank, et. al., "Assessment of plasma power deposition on the ITER ICRH antennas", Nuclear Materials and Energy, Volume 27, 2021, 101021, ISSN 2352-1791,

[12] H. Anand, et al., "Validation of a real-time model-based approach for ITER first wall heat flux control on the TCV tokamak", in: 25th EPS Conf. Plasma Phys., Prague, 2018, p. P2.1074. URL: http://ocs.ciemat.es/EPS2018PAP/pdf/P2.1074.pdf.